

MODELING AND MODEL VALIDATION OF A CHEMICAL INJECTION SPRAYER SYSTEM

K. R. Felizardo, H. V. Mercaldi, P. E. Cruvinel, V. A. Oliveira, B. L. Steward

ABSTRACT. *Efficient control strategies can be used to avoid off-target application in the operation of variable rate application sprayers. The main processes involved in the operation of a variable rate application sprayer are the injection of chemical and its mixing with the carrier. Therefore, the objective of this research was to develop mathematical models for a chemical direct injection system (DIS) including the carrier-chemical mix to assist the design and prediction of the variable rate application errors. The modeling of the DIS involves different engineering fields and is based on the physical parameters of the hydraulic and electrical-mechanical components, fluid equations and experimental procedures.*

The developed models for the chemical DIS were validated via a normalized root mean square error (RMSE) index using a laboratory-scale sprayer test bench built to design sprayers and analyze their performance. These models captured the realistic operation of the chemical injection system including the effect of the transport delay which is dependent on the carrier-chemical mix flow rate. Experimental results of the DIS flow rates and pressure yielded normalized RMSE values lower than 0.4 indicating that the sprayer performance can be efficiently predicted with the developed models. Additionally, experimental curve fitting results for the carrier-chemical mix time constant and transport delay parameters from step changes of the chemical and carrier-chemical flow rates yielded a statistic coefficient of determination R^2 close to 1 indicating that these DIS parameters can be efficiently predicted from experimental step responses.

Keywords. *DIS modeling, Dynamic model development, Model simulation, Transport delay, Variable rate application.*

A wide variety of weeds, insects, and pathogens can cause considerable losses in agricultural production. Crop protection is important to keep the crop yield at profitable levels for a competitive market. To reduce crop losses, growers rely heavily on pesticides. Most of the pesticides, such as herbicides, fungicides, and insecticides have associated risks of environmental contamination and degradation of food quality. Even considering the risks involved in the use of chemicals, large amounts are used in fields around the world every year. Recent studies showed that since 2007, Brazil is the largest consumer of pesticides in the world, and in 2012, about 350,000 tons of pesticides (active ingredient) were applied (Ferreira et al., 2013). Herbicides account for about 60% of these pesticides, since chemical weed control is a common strategy.

The concerns of the public over environmental contamination and food quality have incentivized the agricultural machinery industry and scientific communities to develop methods and equipment for variable rate chemical application as a strategy to more effectively apply chemicals optimally relative to crop plant needs.

Agricultural machinery and technologies are available today that enable variable rate chemical application based on prescription maps or sensors (Sokefeld, 2010). Variable rate application can be performed by varying the formulation rate of the chemical on-the-go using a direct injection system (DIS) (Lammers and Vondricka, 2008). A DIS is an electronically controlled system in which the chemical is injected into the carrier stream. The DIS has separate chemical and carrier reservoirs, and the chemical can be injected into the carrier stream at different locations in the system.

There is evidence that herbicides applied at wrong rates (under or over application) can cause resistance in target plants (Manalil et al., 2011) or environmental contamination. Investigations evaluating application rate errors showed that the errors are not only due to the deviations from the target flow rates, but also due to interaction between the sprayer application control subsystem dynamics and response time (Aissaoui et al., 2011; Steward and Humburg, 2000).

The DIS response time, defined as the time required for the carrier-chemical mix concentration at the last nozzle reach and stay within 2% of its steady-state value, depends on sprayer dynamics and transport delay (Lammers and

Submitted for review in January 2015 as manuscript number ITSC 10606; approved for publication by the Information, Technology, Sensors, & Control Systems Community of ASABE in January 2016.

The authors are **Kleber R. Felizardo**, Prof. Adjoint, Departamento Acadêmico de Elétrica, Universidade Tecnológica Federal do Paraná, Cornélio Procópio, PR; **Heitor V. Mercaldi**, Ph.D Student, Departamento de Engenharia Elétrica, Universidade de São Paulo, São Carlos, SP; **Paulo E. Cruvinel**, Researcher, Embrapa Instrumentação, São Carlos, SP; **Vilma A. Oliveira**, Professor, Departamento de Engenharia Elétrica, Universidade de São Paulo, São Carlos, SP; and **Brian L. Steward**, **ASABE Member**, Professor, Department of Agricultural and Biosystem Engineering, Iowa State University, Ames, Iowa. **Corresponding author:** Vilma A. Oliveira, Universidade de São Paulo, 400 Avenida Trabalhador São-carlense, São Carlos-SP, 13566-590; phone: +55 16 3373-9336; e-mail: vilma@sc.usp.br.

Vondricka, 2010). Transport delay is a function of the flow rate and distance between the injection point and each individual nozzle. A greater distance between the injection point and the nozzles will lead to longer transport delays of chemical concentration changes, but may also lead to greater mixture uniformity. In addition, DIS increase the spraying flexibility as it enables dual control of both carrier and chemical flow rates and simultaneous application of multiple chemicals. However, DIS could also have greater application rate errors in comparison to conventional sprayers.

In past research, efforts were made to mathematically model and characterize a DIS. Steward and Humburg (2000) developed mathematical models of the chemical and carrier sub-systems of the Raven SCS-700 chemical injection system and simulated the performance of various sprayer configurations. In the work by Steward and Humburg (2000), the transport delay effect was minimized by carrier control. In Zhu et al. (1998), the transport delay was modeled and the results showed that it was not affected by the viscosity of the simulated pesticides. Recently, Vondricka et al. (2007) studied the DIS mixing process and characterized the concentration dynamics and Aissaoui et al. (2009) analyzed the concentration dynamics in both serial and parallel boom layouts. In the latter, the concentration dynamics were studied by means of an involving numerical model based on finite volume method with the objective of optimizing the boom layouts to reduce the transport delay.

In the present work, a complete model of a DIS including the dynamics of the carrier-chemical mix concentration was presented. The models for the concentration time constant and transport delay parameters were obtained from measurements of step responses and curve fitting. Therefore, the objectives of this research were to:

1. Obtain a mathematical model for the dynamics of the chemical sub-system of a laboratory-scale DIS sprayer test bench to design appropriate controllers.
2. Model mathematically the dynamics of the carrier-chemical mix sub-system and carrier-chemical mix concentration of the same laboratory-scale DIS.
3. Predict the DIS response time and transport delay to anticipate a map-based application rate to avoid under application.

METHODS AND MATERIALS

A laboratory test bench was designed and built to obtain the presented models. This test bench is part of a facility for research into control systems for site-specific application of chemicals. The performance of the models in accurately describing observed DIS dynamics was measured using the RMSE with a normalization factor. The RMSE index is defined as the ratio:

$$RMSE = \frac{\sqrt{\sum_{k=1}^N [(y(k) - \hat{y}(k))]^2}}{\sqrt{\sum_{k=1}^N [(y(k) - \bar{y})]^2}} \quad (1)$$

where k is the sampling instant, $y(k)$, \bar{y} and $\hat{y}(k)$ are the actual measured outputs, its mean value in the prediction horizon N , and the predicted output, respectively. The RMSE index as defined in equation 1, compares the error obtained from the model to the error obtained with the mean value of the output in the prediction horizon. Therefore, a RMSE value much less than one indicates a superior performance of the predicted output from the model in relation to its mean value. The studied DIS parameters K_v , τ_c , and T_c describing the proportional valve fluid resistance and the time constant and transport delay of the carrier-chemical mix dynamics, respectively, were approximated by mathematical functions obtained by fitting experimental data. They were evaluated by the R-squared (R^2) statistical measure, also known as the coefficient of determination, ranging from 0 to 1. The R^2 measure indicates how close the data are to the fitted function. A R^2 value closer to 1 explains the variability of the experimental data around its mean.

CHEMICAL INJECTION SPRAYER SYSTEM DESCRIPTION

The chemical application system model developed in this work uses DIS technology with the injection point located upstream from the sprayer pump as in Tompkins et al. (1990), Antuniassi et al. (2002), Sui and Thomasson et al. (2003), and Gillis et al. (2003). The application system is composed of the chemical injection and carrier-chemical mix sub-systems (fig. 1). The system transport delay and time response are related to the carrier-chemical mix and chemical flow denoted q_m and q_c , respectively. These flows are controlled to give the target carrier-chemical mix concentration denoted c_r , which defined as:

$$c_r = \frac{Q_{cr}}{Q_{mr} - Q_{cr}} \quad (2)$$

where Q_{mr} is the reference carrier-chemical mix volume flow rate and Q_{cr} , is the reference chemical volume flow rate, both in $L \text{ min}^{-1}$, which are calculated as follows (Shiratsuchi and Fontes, 2002):

$$Q_{mr} = \frac{D_{mr} v_t e_n n}{60,000} \quad (3)$$

$$Q_{cr} = \frac{D_{cr} v_t e_n n}{60,000} \quad (4)$$

where D_{cr} and D_{mr} are the chemical application and the carrier-chemical mix application reference rates, respectively, given in $L \text{ ha}^{-1}$, taken from map of requested application rates, e_n is the nozzle spacing in cm, n is the number of nozzles, and v_t is the tractor ground speed in km h^{-1} . Now, since $Q_{mr} \gg Q_{cr}$, we can simplify equation 2 to:

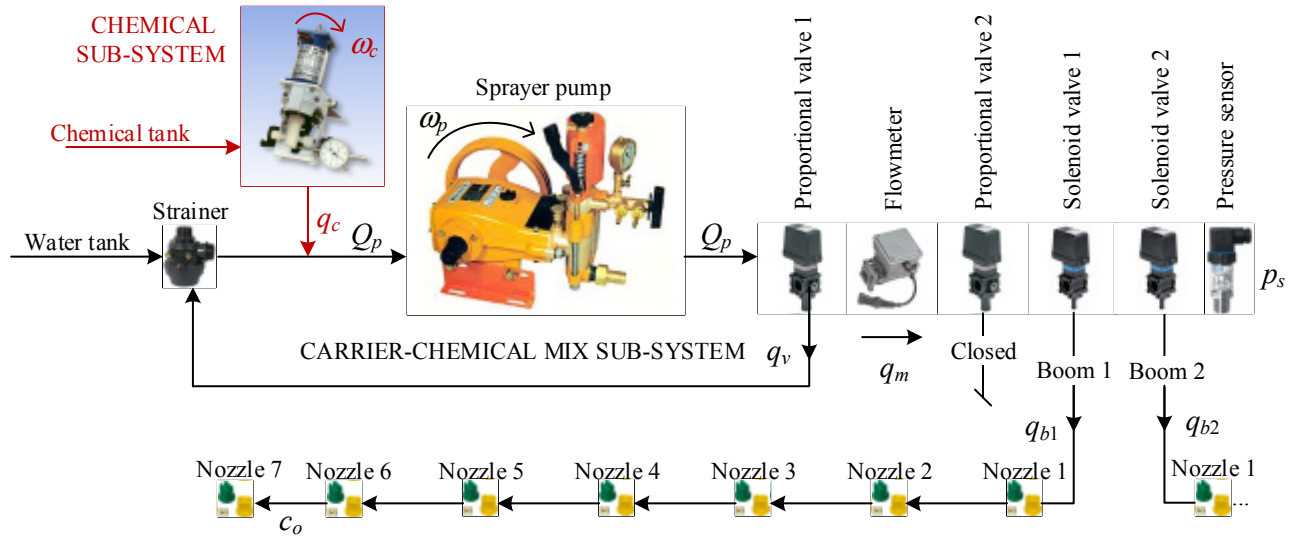


Figure 1. Schematic diagram of the chemical injection sprayer system consisting of chemical and carrier-chemical mix sub-systems.

$$c_r = \frac{Q_{cr}}{Q_{mr}} \quad (5)$$

The test bench chemical sub-system consisted of a 30 L chemical tank and a variable stroke (manually adjustable) positive displacement piston pump with a maximum flow rate $2,304 \times 10^{-3} \text{ L min}^{-1}$ and maximum working pressure of 100 kPa (model QB-3, Fluid Metering Inc., Syosset, N.Y.). The pump was powered by a 12 V DC motor that could draw up to 4 A. The tank had a reed-switch-based level sensor (model CBN, Contech, São Paulo, SP). The chemical flow (q_c) was experimentally found to be proportional to the motor shaft speed (ω_c) across a range of operating pressures. A 1024 line incremental encoder (model HTR-W2-1024-3-PP, Metaltex, São Paulo, SP) was used to measure ω_c .

The carrier-chemical mix sub-system of the test bench was composed of a 300 L water tank, a sprayer pump, four electrohydraulic valves, a flow meter, two pressure sensors, spray nozzles, and hose pipelines. The water tank had reed-switch maximum and minimum level sensors. The carrier pump (model MB-42, Jacto, Pompéia, SP) was a three piston fixed positive displacement pump with a maximum flow rate of 42 L min^{-1} and maximum pressure of 3400 kPa which was driven by a three-phase, four-pole 60-Hz 2.2-kW induction motor (model 90L, Kohlbach, São Paulo, SP). The sprayer pump flow (Q_p) was experimentally found to be proportional to the induction motor angular shaft speed (ω_p). The motor shaft speed was regulated by a frequency inverter (model VFD022B23A, Delta Electronics, São Paulo, SP), which was set to turn the carrier pump at its rated rotational speed of 800 rev min^{-1} . The set of four electrohydraulic valves consisted of two proportional spray control valves and two solenoid boom section valves (models 463020S and 463001S, respectively, Arag, Pinhais, PR). Each valve had three ports in a tee topology which enabled flow to enter through one side of the tee with controlled flow exiting through the bottom part of the tee. The flow was controlled

by a rotating needle valve mechanism turned by a 12 V/0.5 A DC motor. The solenoid valves were used to split the carrier-chemical mix between two spray booms numbered 1 and 2 with boom flows denoted q_{b1} and q_{b2} . Each of the two spray booms had 3.5 m with seven five-way nozzle holders equally spaced. Each nozzle holder contained five 110° standard (ISO 10625) flat fan ceramic nozzle (models 422SFC110-02(03, 04, 05, 06), Arag, Pinhais, PR). An electromagnetic flow meter (model 4621AA30000, Arag, Pinhais, PR) was used to measure the flow-rate of the mixture, q_m , working in the range of 5 to 100 L min^{-1} with maximum full scale error of 1%. A 1024 line encoder was used to measure the needle position, θ_v , of the proportional valve 1 (fig. 1). A second proportional valve (#2 in fig. 1) was used to obtain different values for the flow (q_m) and pressure (p_s) to model the fluid resistance of proportional valve 1 as described later. A pressure sensor (model A-10, Wika, Iperó, SP) measured the pressure (p_s) at the valve stack, working in the range 0 to 600 kPa with maximum full scale error of 1%.

TEST BENCH INSTRUMENTATION

The liquid chemical application test bench (fig. 2) with a DIS described above and illustrated in figure 1 was designed and built in a shared facility between Embrapa Instrumentação and the Laboratório de Controle, Escola de Engenharia de São Carlos (Cruvinel et al., 2011). A programmable automation controller (PAC) (model cRIO-9073, National Instruments, São Paulo, SP) was used for control and data acquisition of the test bench (National Instruments, 2010).

The controller combined an embedded 266 MHz real-time processor and a user-programmable FPGA chip with 2 million user programmable gates within a single chassis supporting up to eight I/O modules (National Instruments, 2010). The FPGA was connected to the processor through a high speed PCI bus and each I/O module was also connected to the FPGA.

PAC firmware was developed in the LabVIEW graphical programming language (version 2009, National



Figure 2. Front view of the test bench assembled in laboratory scale. In the background, the control panel with electronics, electro-mechanical and hydraulic components is shown. In the front, details of the booms with spray nozzles and the conveyor belt for analysis of droplets using water sensitive paper are shown (Cruvinel et al., 2011).

Instruments, São Paulo, SP), and the algorithms were implemented in the LabVIEW PC, LabVIEW Real-Time and the LabVIEW FPGA platforms. The real time processor deterministically executed the algorithms developed for the LabVIEW RT embedded application. The FPGA chip simultaneously executed the algorithms created in the LabVIEW FPGA software (fig. 3). The program developed for the LabVIEW PC managed user interaction for the operation and application setting of the system mounted on the test bench, including visualization and data storage during the tests. The data sampling rate was 20 Hz. The mathematical models developed in this work were simulated on the LabVIEW PC.

MODELING THE CHEMICAL SUB-SYSTEM

A chemical injection mathematical model was developed to describe the dynamic behavior of the chemical flow rate (q_c) (Mercaldi et al., 2011). The dynamics of the chemical sub-system is given by a DC motor coupled to a displacement pump used as an injection pump (fig. 4). The load torque varied linearly with the pressure denoted p_c at the injection pump output, and the flow (q_c) varied linearly with the angular speed (ω_c) (Akers et al., 2006). The power amplifier driving the DC motor delivered a chopper pulse-width-modulation (PWM) signal and was modeled as a gain denoted K_{pt} . The chopper PWM was implemented with a power transistor operating in saturation and cut-off with a switching frequency of 500 Hz. The transistor was driven by the duty-cycle of the PWM signal denoted d_c which was generated in response to the speed error. The armature current and voltage are denoted i_c and v_c , respectively.

The DC motor and flow were described mathematically as:

$$L_c \frac{di_c}{dt} + R_c i_c + K_e \omega_c = K_{pt} d_c \quad (6)$$

$$J \frac{d\omega_c}{dt} + b\omega_c + K_p p_c = K_t i_c \quad (7)$$

$$q_c = K_p \omega_c \quad (8)$$

where K_t is the torque constant, K_e is the back electromotive force constant, R_c is the armature resistance, L_c is the armature inductance, J is the moment of inertia of the motor rotor, b is the viscous friction coefficient in the motor bearing shaft, and K_p is the volumetric displacement of the piston pump.

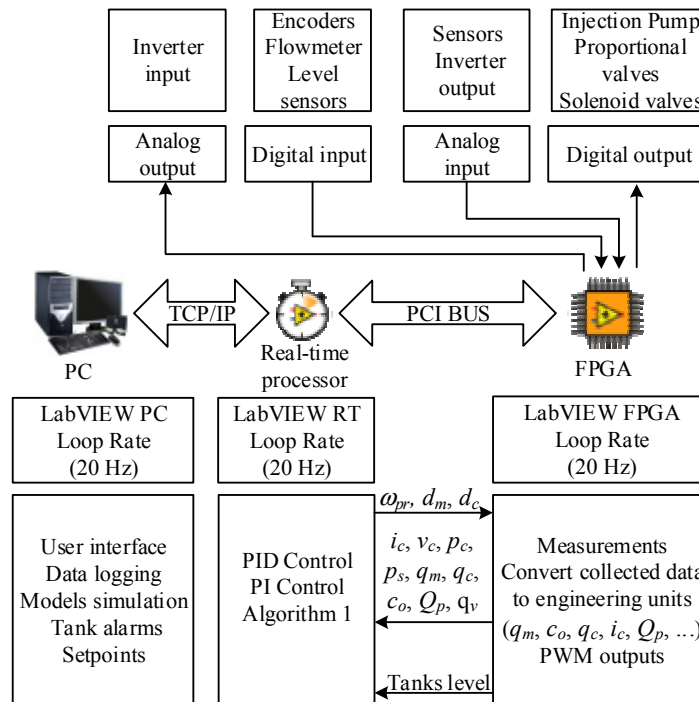


Figure 3. The automation system developed consisted of three platforms: the FPGA, the real time, and the PC platforms.

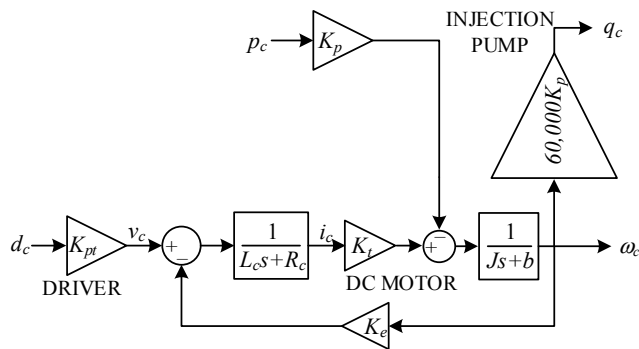


Figure 4. Block diagram of the chemical sub-system.

Experimental Procedures

The chemical sub-system model may be obtained by standard procedures such that it describes the behavior of the chemical flow rate (q_c). To estimate the parameters of the chemical injection sub-system model, an experimental system was built which included the DC motor, the injection pump, pressure sensor, and a manually actuated common two-way valve connected to the pump outlet (fig. 5).

A regulated DC voltage source was used to set the DC motor armature voltage (v_c). The reference injection pressure (p_c) was set in the range of 0 to 400 kPa by manually opening the two-way valve connected to the pump output. A Hall effect current sensor (model ACS712, Allegro MicroSystems, Minneapolis, Minn.), a pressure sensor (model A-10, Wika, Iperó, SP), and an incremental encoder (model HTR-W2-1024-3-PP, Metaltex, São Paulo, SP) were used to measure the current (i_c), pressure (p_c), and speed (ω_c), respectively. The cRIO-9073 PAC was used to acquire data every 10 ms for i_c , v_c , p_c , and ω_c . The gradient descent method was used to estimate the model parameters using the Simulink Parameter Estimation tool available in Matlab (vers. R2012a, The Mathworks, Natick, Mass). In this experiment, an identification procedure based on output measurements was accomplished as follows. During the first 50 seconds, the input voltage of the DC motor v_c was randomly varied using a potentiometer to fully excite the output. After this time, the pressure (p_c) was also varied randomly by manually opening and closing a two-way valve.

MODELING OF THE CARRIER-CHEMICAL MIX SUB-SYSTEM

The modeling of the carrier-chemical mix sub-system involves different engineering fields and is based on

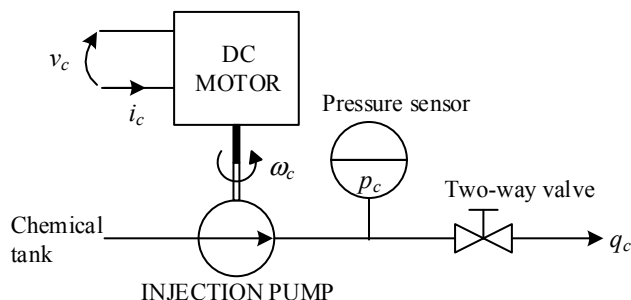


Figure 5. Chemical sub-system setup for data acquisition.

physical parameters of the hydraulic components, basic mechanical fluid equations and two experimental procedures. The experimental procedures are designed to obtain the equivalent pumping resistance (K_{pn}) and the proportional valve fluid resistance (q_c) using a flow meter and pressure sensors. Therefore, the parameters obtained experimentally are dependent on the accuracy of the measurements and this will impact the obtained nominal values of the parameters.

The hydraulic model of the carrier-chemical mix sub-system describes the dynamic behavior of both the system pressure (p_s) and the carrier-chemical mix flow rate (q_m). The carrier-chemical mix sub-system includes the following components: a pump set, the electrohydraulic proportional and solenoid valves, sprayer nozzles and hoses.

Pressure System Dynamics

The pressure-flow relationship of the valves and nozzles were modeled as orifices with turbulent flow (Garcia, 2005; Merritt, 1967):

$$\Delta p = K_0 q^2 \quad (9)$$

where Δp is the pressure drop across the nozzle, q is the orifice volumetric flow rate, and K_0 is the fluid resistance of the orifice. The fluid resistance parameters of this sub-system were obtained either experimentally, by measuring Δp and q , or were obtained from manufacturer catalogs. In figure 6, the nozzle, the flow meter, the valves, and conduit of the hydraulic circuit of the chemical injection sprayer system are represented by fluid resistances (Akers et al., 2006).

The following model assumptions were made:

- each of the sprayer nozzles has the same fluidic resistance (K_n);
- the equivalent fluidic resistance of each boom (K_{pn}) which captures the effect of the plumbing between nozzles is the same;
- the fluidic resistances (K_{vs}) of each solenoid valve is the same;
- the fluidic resistance (K_{pb}) of the pipes connecting each solenoid valve to the first nozzle of each boom is the same; and
- the fluidic resistance (K_f) of the flow meter is negligible.

Therefore, it can be assumed that the carrier-chemical mix flow (q_m) is divided equally between the two booms:

$$q_{b1} = \frac{q_m}{m} \quad (10)$$

where q_{b1} is the volume flow-rate of boom 1, and m is the number of booms. According to the configuration of the hydraulic circuit shown in figure 6, the pressure (p_s) is given by the sum of pressures, that is,

$$p_s = \Delta p_{vs} + \Delta p_{pb} + \Delta p_{pn} + \Delta p_n \quad (11)$$

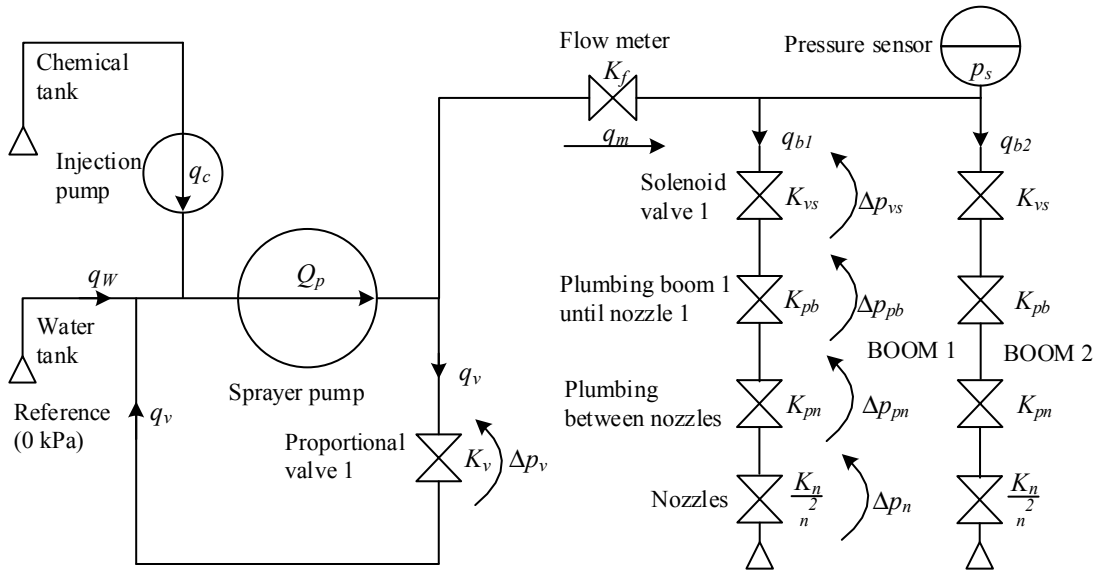


Figure 6. Equivalent hydraulic circuit of the chemical injection sprayer system.

where Δp_{vs} is the pressure drop across solenoid valve 1, Δp_{vb} is the pressure drop in the section pipe which extends from the output solenoid valve 1 until the first spray nozzle 1, Δp_{vn} is the pressure drops due pipes between the sprayer nozzles, and Δp_n is the pressure drop across the nozzles. The pressure drop Δp_{vs} is:

$$\Delta p_{vs} = \frac{K_{vs}}{m^2} q_m^2 \quad (12)$$

The pressure drop (Δp_{pb}) in the fluid conduit connecting the boom solenoid valve to the first nozzle was calculated using Darcy's equation:

$$\Delta p_{pb} = \frac{K_{pb}}{m^2} q_m^2 \quad (13)$$

where $K_{pb} = \frac{fL\rho}{2d_i A^2}$ with L the length of the pipe which extends from the output solenoid valve 1 until the first sprayer nozzle of boom 1, d_i the internal diameter of this pipe with internal area (A), f the friction factor, ρ is the mass density of the fluid.

The pressure drop (Δp_{pn}) is given by:

$$\Delta p_{pn} = \frac{K_{pn}}{m^2} q_m^2 \quad (14)$$

Finally, the pressure drop (Δp_n) in the sprayer nozzles is:

$$\Delta p_n = \frac{K_n}{n^2} \frac{q_m^2}{m^2} \quad (15)$$

where K_n divided by n^2 captures the effect of the n nozzles operating in parallel. The system pressure (p_s) is thus obtained by replacing equations 12, 13, 14, and 15 in equation 11 yielding:

$$p_s = \frac{K_{eq}}{m^2} q_m^2 \quad (16)$$

with K_{eq} the equivalent fluidic resistance given by:

$$K_{eq} = K_{vs} + K_{pb} + \frac{K_{pn}}{n^2} + K_n$$

Carrier-Chemical Mix Flow Dynamics

The carrier-chemical mix flow q_m is regulated in the proportional valve 1 through the return flow rate (q_v). Considering the sprayer pump flow rate (Q_p) it follows that:

$$q_v = Q_p - q_m \quad (17)$$

The pressure drop (Δp_v) in the proportional valve 1 is given by:

$$\Delta p_v = K_v q_v^2 \quad (18)$$

with K_v the fluid resistance of the proportional valve 1. Substituting equation 17 into equation 18 for q_v results in:

$$\Delta p_v = K_v Q_p^2 - 2K_v Q_p q_m + K_v q_m^2 \quad (19)$$

From the hydraulic circuit configuration (fig. 6), it follows that:

$$\Delta p_v = p_s - K_f q_m^2 \quad (20)$$

The electromagnetic flow meter fluid resistance (K_f) was neglected. Thus,

$$\Delta p_v = p_s \quad (21)$$

Therefore, from equation 16 and 19 it follows:

$$(K_v - K_{eq}) q_m^2 - 2K_v Q_p q_m + K_v Q_p^2 = 0 \quad (22)$$

which yields:

$$q_m = \frac{Q_p \left(\sqrt{K_{eq} K_v} - K_v \right)}{K_{eq} - K_v} \quad (23)$$

The carrier-chemical mix flow given by equation 23 depends on the proportional valve fluidic resistance (K_v), which is a function of the needle rotation angle (θ_v) of the proportional valve 1. The needle angle (θ_v) is coupled to the DC motor of proportional valve 1. This motor is driven by a power amplifier consisting of an H-bridge controlled by a duty-cycle of a PWM signal. The DC motor is represented by a first order system plus an integrator with a gain K_m and a time constant T_m . Additionally, the motor responds only to a certain range of duty cycles. Let d_m be selected according to the duty cycle denoted d as follows: if the valve is opening $d_m = -d$ and if it is closing $d_m = d$. Now, consider that the H-bridge DC motor driver is modeled by a dead band type with saturation nonlinearity and a gain K_{ph} . This nonlinearity is expressed by the function $DZ(d_m)$:

$$DZ(d_m) = \begin{cases} D_+ & \text{if } d_m > D_+ \\ k_+(d_m - d_+) & \text{if } d_+ < d_m \leq D_+ \\ 0 & \text{if } d_- \leq d_m \leq d_+ \\ k_-(d_m - d_-) & \text{if } d_- < d_m \leq D_- \\ D_- & \text{if } d_m < D_- \end{cases} \quad (24)$$

where $[d_- d_+]$ is the dead band, D_- and D_+ the saturation limits of d_m , and k_- and k_+ are the adjustment parameters for the slope gains. The DC motor and driver of proportional valve 1 can thus be described as:

$$T_m \frac{d^2}{dt^2} \theta_v + \frac{d}{dt} \theta_v = K_m K_{ph} DZ(d_m) \quad (25)$$

Figure 7 shows the DC motor and driver model in form of block diagram.

Experimental Procedures

The nozzle fluid resistance (K_n) was obtained via the flow-pressure curve provided by the manufacturer and the solenoid valve resistance (K_{vs}) was given by the manufacturer. The resistance in the boom conduit from the solenoid valve to the first nozzle (K_{pb}) was calculated using equation 13 with the physical parameters of the pipe and fluid L , d_b , f , and of the fluid (ρ).

The equivalent pumping resistance (K_{pn}) was obtained experimentally by measuring the mixture flow rate (q_m) and the pressure drop between the first and the last nozzle of boom 1 for five different flow rates (15, 20, 25, 30, and 35 L min⁻¹). These data were fit to equation 14 to determine the fluid resistance (K_{pn}). The parameters K_{ph} , K_m , T_m , and $[d_+, d_-]$ were obtained via a position step response experiment for a duty cycle, $d=100\%$ and again, the

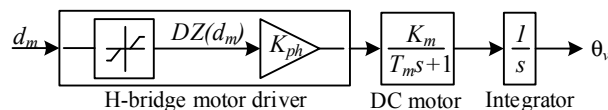


Figure 7. Block diagram of the control valve DC motor and driver.

gradient descent method via the Simulink Parameter Estimation tool was used. The parameter (Q_p) is the maximum flow rate of the sprayer pump which was provided by the manufacturer. The proportional valve fluid resistance (K_v) as a function of the valve stem angle (θ_v) was obtained experimentally by measuring the carrier-chemical mix flow rate (q_m) and the valve block pressure (p_s) for different valve stem angles (θ_{vi} , $i = 1 \dots 14$) (Steward and Humburg, 2000). During the experiment, the solenoid valves 1 and 2 in figure 1 remained closed. Slowly the proportional valve 2, initially fully opened, was turned toward the closed position until the pressure (p_s) at the output of the proportional valve 1 reached 700 kPa. Then, the proportional valve 2 was returned to the fully open position and the proportional valve 1, initially at position fully opened denoted θ_{v1} was set to the next position. This procedure was repeated for each angle (θ_{vi} , $i = 2 \dots 14$). For each angle (θ_{vi}) a constant (K_{vi} , $i = 1 \dots 14$) was calculated by linear fitting of q_m^2 versus p_s . The physical parameters of the carrier-chemical mix sub-system are given in table 1.

The open loop carrier-chemical mix sub-system is marginally stable because of the presence of an integrator (see fig. 7), and hence a proportional gain controller $K_c = 20$ was designed to stabilize the closed loop system (fig. 8).

The cRIO-9073 PAC was used to collect flow and pressure (q_m , p_s) data, and a user interface was created in the LabVIEW PC for viewing and storing data every 50 ms. The proportional controller was developed in the LabVIEW RT software and had a 50 ms control loop.

THE CARRIER-CHEMICAL MIX CONCENTRATION MODEL

The dynamic response of the carrier-chemical mix concentration at the last nozzle denoted c_o , was modeled using a first order linear model with transport delay (Ogata, 2010):

$$T_c \frac{d}{dt} c_o + c_o = K c_i (t - \tau_c) \quad (26)$$

where K is the static gain, τ_c is the transport delay, T_c is the system time constant, and c_i is the concentration at the

Table 1. Carrier-chemical mix sub-system physical parameters.

Saturations limits (eq. 24), $[D_+, D_-]$	[100,-100]
Pipe length, L	1.35 m
Pipe internal diameter, d_i	1.27×10^{-2} m
Friction factor, f	8.2×10^{-3}
Mass density, ρ	1.0×10^{-3} kg m ⁻³
Number of booms, m	2
Number of nozzles per boom, n	7
Sprayer pump volumetric flow rate, Q_p	42.00 L min ⁻¹
Proportional gain controller, K_c	20

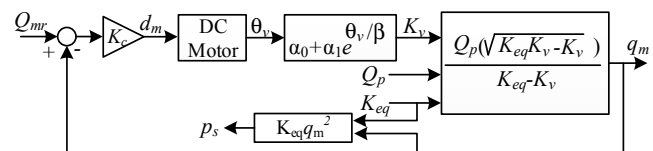


Figure 8. Block diagram of the carrier-chemical mix sub-system with the proportional controller.

injection point located upstream from the sprayer pump and is given by:

$$c_i = \frac{q_c}{q_m} \quad (27)$$

The Sundaresan and Krishnaswamy method (1978) can be used to find the parameters K , τ_c , and T_c from the step response with a step input (c_i). Their method uses the time taken to reach 35.3% denoted $t_{35.3}$ and to reach 85.3% $t_{85.3}$ of the steady state step response denoted c_o . The parameters are given by:

$$\tau_c = 1.2t_{35.3} - 0.29t_{85.3} \quad (28)$$

$$T_c = 0.69(t_{35.3} - t_{85.3}) \quad (29)$$

and
$$K = \frac{\Delta c_o}{\Delta c_i} \quad (30)$$

The parameter τ_c is the time required to transport any concentration changes to the last nozzle. The following function for the transport delay τ_c is proposed:

$$\tau_c = K_1 q_m^{-\phi_1} \quad (31)$$

with model parameters K_1 and ϕ_1 . Also, the following function for the time constant T_c is proposed:

$$T_c = K_2 q_m^{-\phi_2} \quad (32)$$

with K_2 and ϕ_2 constants. Figure 9 presents the block diagram of the carrier-chemical mix concentration model.

The system time response (t_s) may be estimated from the time constant T_c and delay τ_c as follows (Ogata, 2010):

$$t_s = 4T_c + \tau_c \quad (33)$$

where $4T_c$ is the time the carrier-chemical mix concentration (c_o) takes to reach 98% of its steady state value. Replacing equations 31 and 32 in equation 33, it yields:

$$t_s = 4K_2 q_m^{-\phi_2} + K_1 q_m^{-\phi_1} \quad (34)$$

Equations 26 to 34 hold for $q_- \leq q_m \leq q_+$. The value q_- is the minimum value provided by the flow meter, and q_+ is the maximum sprayer pump flow rate.

Experimental Procedures

The electrical conductivity was used to estimate the carrier-chemical mix concentration on the validation phase of the model, that is, to estimate the total amount of solids

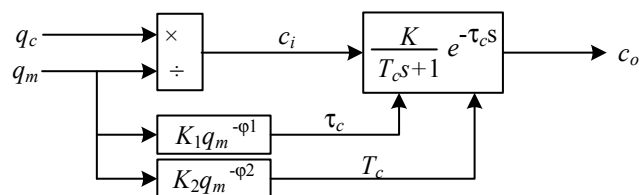


Figure 9. Block diagram of the carrier-chemical mix concentration model.

dissolved in water, which stands for total dissolved solids. The electrical conductivity of the water depends on the water temperature and, for calibration, the temperature equal to 25°C was standardized. However, while the electrical conductivity is a good indicator of the total salinity, it still does not provide any information about the ion composition in the water. The commonly used unit for measuring electrical conductivity of water is $\mu\text{S}/\text{cm}$, and a known solution of sodium chloride (NaCl) was used. The electrical conductivity is a measure of the capacity of water to conduct electrical current, it is directly related to the concentration of salts dissolved in water, and therefore to the total dissolved solids. Salts dissolve into positively charged ions and negatively charged ions, which conduct electricity. Since it is difficult to measure the total dissolved solids in real pesticides, during the validation procedures, the electrical conductivity of the water was used as a measurement. Nevertheless, when the salt concentration reaches a certain level, electrical conductivity is no longer directly related to salts concentration. This is because ion pairs are formed. Ion pairs weaken each other's charge, such that above this level, higher total dissolved solids will not result in equally higher electrical conductivity.

The variation of the conductivity was measured with a conductivity sensor (model INPRO-7108, Mettler Toledo, Barueri, SP) installed near the last nozzle of boom 1. It was placed at this location to consider the worst case for estimating the response time and transport delay of the direct injection system.

RESULTS AND DISCUSSION

ESTIMATING AND VALIDATING THE PARAMETERS OF THE CHEMICAL SUB-SYSTEM

Based on the setup described in figure 5, the parameters of chemical sub-system modeled in figure 4 were estimated experimentally. The obtained results are shown in table 2. The pump displacement (K_p) was provided by the manufacturer and the gain (K_{pi}) was set as the theoretical power amplifier gains which are also shown in table 2.

To validate the model, a new set of experimental data was obtained using the setup showed in figure 5 already described. The experimental DC motor responses i_c and ω_c were used to compare the responses of the simulated model using Simulink as shown in figure 10. Also, the model inputs, pressure and voltage used are shown. The flow rate q_c was obtained via equation 8.

The RMSE values of the chemical sprayer sub-system predicted variables ω_c , q_c , and i_c were 0.31, 0.31, and 0.83, respectively. The RMSE values for ω_c and q_c were less than 0.4 indicating very good performance whereas the RMSE value for the current i_c is more than 0.8 indicating the prediction is not as good as ω_c and q_c with 0.31 RMSE. The reason for this is that the DC motor current has a fast time constant. However, as the regulated variable is the motor speed and not the torque, the flow rate model response followed the dynamics of the chemical sub-system and the model can be used to efficiently predict the flow rate behavior.

Table 2. Chemical sub-system parameters.

Parameter Name and Variable	Value
Armature resistance, R_c	$6.86 \times 10^{-1} \Omega$
Armature inductance, L_c	$1.00 \times 10^{-3} \text{ H}$
Valve motor torque constant, K_t	$3.75 \times 10^{-2} \text{ N m A}^{-1}$
Valve motor back voltage constant,	$3.75 \times 10^{-2} \text{ V s rad}^{-1}$
Valve motor moment of inertia, J	$4.74 \times 10^{-4} \text{ Kg m}^2$
Valve motor damping constant, b	$4.59 \times 10^{-4} \text{ Kg m}^2 \text{ s}^{-1}$
Volumetric displacement of the pump, K_p	$2.07 \times 10^{-7} \text{ m}^3 \text{ rad}^{-1}$
Power amplifier gain, K_{pt}	1.20×10^{-1}

ESTIMATING AND VALIDATING THE PARAMETERS OF THE CARRIER-CHEMICAL MIX SUB-SYSTEM

The models for the pressure and carrier-chemical mix flow dynamics were described in the section methods and materials. The carrier-chemical mix sub-system parameters obtained experimentally are shown in table 3.

Based on the characteristic of the experimental data showed in figure 11, the following function for the fluid resistance K_v was proposed:

$$K_v = \alpha_0 + \alpha_1 e^{\frac{\theta_v}{\beta}} \quad (35)$$

The mathematical model shown in figure 8 was simulated in the Simulink environment using the parameter values given in table 3. The experimental and simulation results for the sprayer nozzles 11003 and 11005 are shown in figure 12. The reference flow rates (Q_{mr}) were determined to cover the range of the working pressure of these spray nozzles which lies between 100 and 500 kPa.

Notice the good approximation of the carrier-chemical mix mathematical model with the actual process response in figure 12. With the 11003 nozzle, the model is under-predicting the low flow rate (~6 L/min) by about 10%, but is very accurate for the other cases. For the 11005 nozzle, a trend was observed of over-estimating the flow rate as the

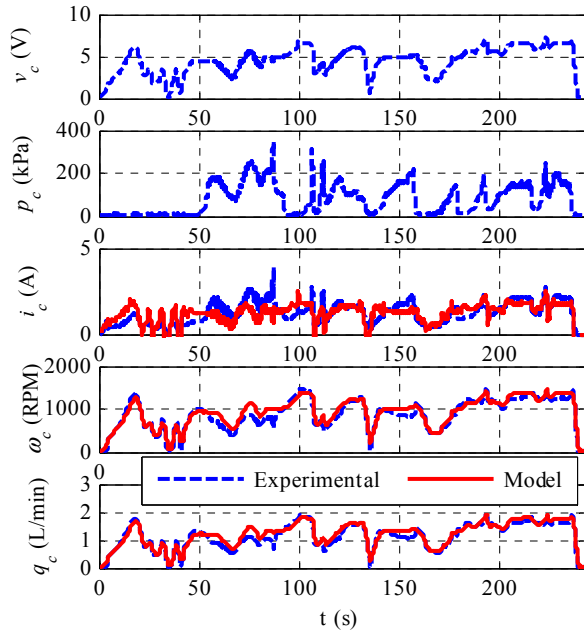


Figure 10. Simulation and experimental results for the chemical sub-system.

Table 3. Carrier-chemical mix sub-system parameters obtained experimentally.

Parameter Name and Variable	Value
Nozzle 11003 fluid resistance, K_n	$2.07 \times 10^2 \text{ kPa (L min}^{-1}\text{)}^{-2}$
Nozzle 11005 fluid resistance, K_n	$0.75 \times 10^2 \text{ kPa (L min}^{-1}\text{)}^{-2}$
Solenoid valve fluid resistance, K_{vs}	$4.08 \times 10^{-2} \text{ kPa (L min}^{-1}\text{)}^{-2}$
Plumbing boom 1 until nozzle 1 fluid resistance, K_{pb}	$4.53 \times 10^{-2} \text{ kPa (L min}^{-1}\text{)}^{-2}$
Equivalent plumbing between nozzles fluid resistance, K_{pn}	$1.35 \times 10^{-2} \text{ kPa (L min}^{-1}\text{)}^{-2}$
Carrier-chemical subsystem equivalent fluid resistance (eq. 16), $K_{eq-11003}$	$4.32 \text{ kPa (L min}^{-1}\text{)}^{-2}$
Carrier-chemical subsystem equivalent fluid resistance (eq. 16), $K_{eq-11005}$	$1.63 \text{ kPa (L min}^{-1}\text{)}^{-2}$
H-bridge gain, K_{ph}	1.20×10^{-1}
Proportional valve motor torque constant, K_m	1.10 rad V^{-1}
Proportional valve motor time constant, T_m	$5.00 \times 10^{-2} \text{ s}$
Proportional valve fluid resistance, K_v	$2.99 \times 10^{-2} \text{ kPa (L min}^{-1}\text{)}^{-2}$
Dead band limits (eq. 24), $[d_+, d_-]$	[20, -20]
Gains (eq. 24), $[k_+, k_-]$	[1.25, -1.25]
Coefficient (eq. 35), α_0	$2.99 \times 10^{-2} \text{ kPa (L min}^{-1}\text{)}^{-2}$
Coefficient (eq. 35), α_1	$2.81 \times 10^{-6} \text{ kPa (L min}^{-1}\text{)}^{-2}$
Coefficient (eq. 35), β	6.53 rad

measured flow rate increases. The difference between simulated and measured data before 20 s could be explained by the full-scale sensor's errors as the error increases when pressure and flow rate are close to their minimum working range.

The normalized RMSE values for the prediction of q_m and p_s using nozzles 11003 and 11005 are shown in table 4. These values are much less than one indicating good performance.

In practice, it is interesting to have simplified experiments to obtain the carrier-chemical mix sub-system model. However, the complete model given is useful to design simplified experiments for model based control for variable rate application. Also, it is useful for comparison purposes.

ESTIMATING AND VALIDATING THE PARAMETERS OF THE CHEMICAL-CARRIER MIX CONCENTRATION MODEL

The determination of the mix concentration model proposed in figure 9 is based on the flow rate q_m , q_c , and measurements of the concentration c_o . The results in this article were obtained with an electrical conductivity meter. In case ionization compounds are not present, other

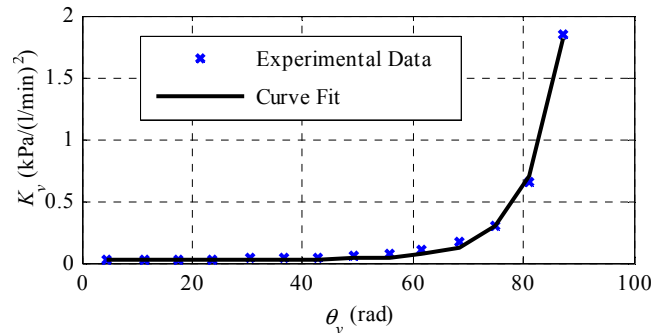


Figure 11. Curve K_v vs. θ_v of the proportional valve 1 found with statistic coefficient of determination $R^2=0.98$.

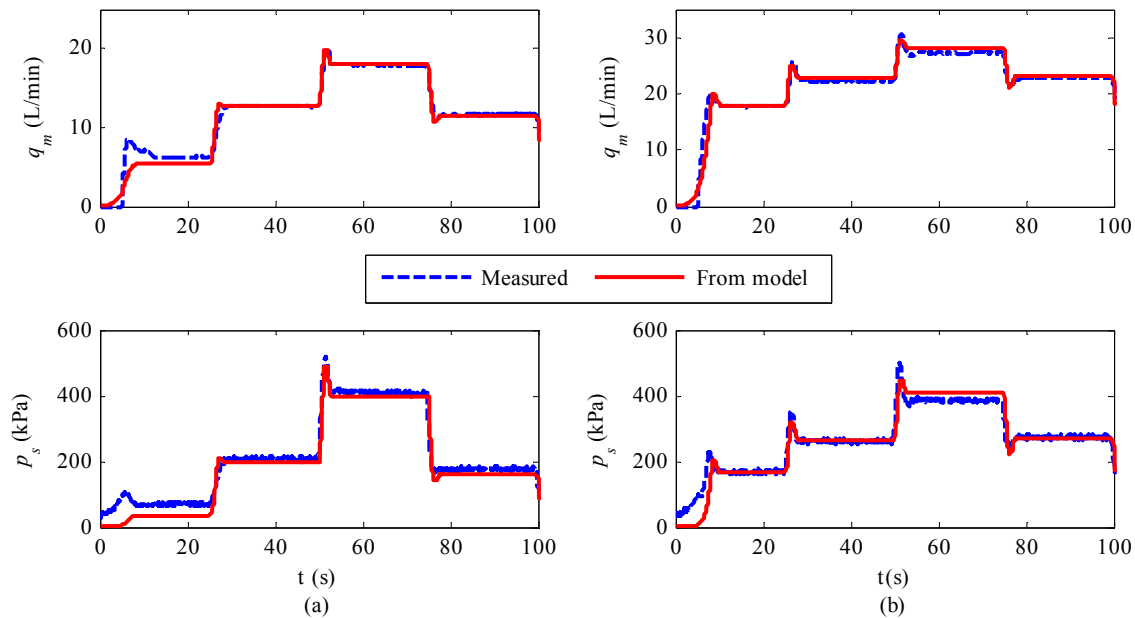


Figure 12. Simulation and experimental results for the carrier-chemical mix sub-system obtained with the feedback control system described in figure 8 with: (a) nozzle 11003 and (b) nozzle 11005.

Table 4. Normalized RMSE values for predicted q_m and p_s .

	q_m	p_s
Nozzle 11003	0.17	0.23
Nozzle 11005	0.16	0.23

methods to measure the concentration should be considered, such as fluorescence based methods (Aissaoui, 2015). From absorbance results, Luck et al. (2012) found that drinking tap water can be used to simulate the sprayer carrier as opposed to deionized (DI) water.

Carrier-chemical mixture conductivity measurements were used to experimentally determine the system response time to step changes of the chemical and carrier-chemical volume flow rates (Antuniassi et al., 2002). The chemical reservoir was filled with 16 L of water containing 50 g of sodium chloride (NaCl). This solution, when injected into the suction line of the sprayer pump through the spray injection pump makes the electrical conductivity of the carrier-chemical mix concentration to vary depending on the salt concentration. Similar experimental procedures to characterize the transient concentration using NaCl were adopted in Downey et al. (2006) and Hoogterp (2009). Zhu et al. (1998), Vondricka et al., (2007), and Aissaoui et al. (2009) evaluated that the viscosity does not affect the transport delay, but affects the concentration transient.

The system response time were obtained with the sprayer booms 1 and 2 in operation. The dynamics of the carrier-chemical mix concentration was evaluated for four cases presented in table 5. For cases I to IV (table 5), the flow q_m was first set, then the set point for the carrier-chemical mix concentration c_r (eq. 5), was set constant at 0.03 for a period of time and after that zeroed. For example, in case I, the initial carrier-chemical mix flow was fixed at 11 L/min, after 30 seconds, salted water at 0.33 L/min was applied for 120 seconds and then the salted water flow was zeroed and the carrier-chemical mix was only water again.

From the system response time for cases (I) to (IV) shown in figure 13, the parameters K , τ_c , and T_c were identified via the Sundaresan and Krishnaswamy method. Table 6 presents the obtained values.

The curve τ_c versus q_m showed in figure 14 obtained from the experimental data given in tables 5 and 6 were used to estimate the parameters K_1 and ϕ_1 in equation 31. Similarly, the curve T_c versus q_m shown in figure 15 were used to estimate parameters K_2 and ϕ_2 in equation 32. The parameters of the carrier-chemical mix concentration model obtained are shown in table 7. The coefficient of determination (R^2) was used to evaluate the proposed functions to describe K_v , τ_c , and T_c shown in figures 11, 14, and 15.

Experimental data were collected to validate the mathematical model for the carrier-chemical mix concentration. Again, the cRIO-9073 PAC was used to collect the data for the carrier-chemical mix concentration c_o and a user interface was developed in the LabVIEW PC software for viewing and acquiring data every 50 ms. The block diagram of the mathematical model obtained is

Table 5. Case studies to estimate the carrier-chemical mix concentration model parameters.

Cases	q_m (L min ⁻¹)	q_c (L min ⁻¹)
I	11.00	0.33
II	17.00	0.51
III	23.00	0.69
IV	29.00	0.87

Table 6. Values of the parameters K , τ_c , and T_c identified from the process responses in figure 13.

Cases	K		
	(mS cm ⁻¹)	τ_c (s)	T_c (s)
I	5120	23.04	19.27
II	5120	16.04	12.11
III	5120	10.86	9.50
IV	5120	9.27	7.50

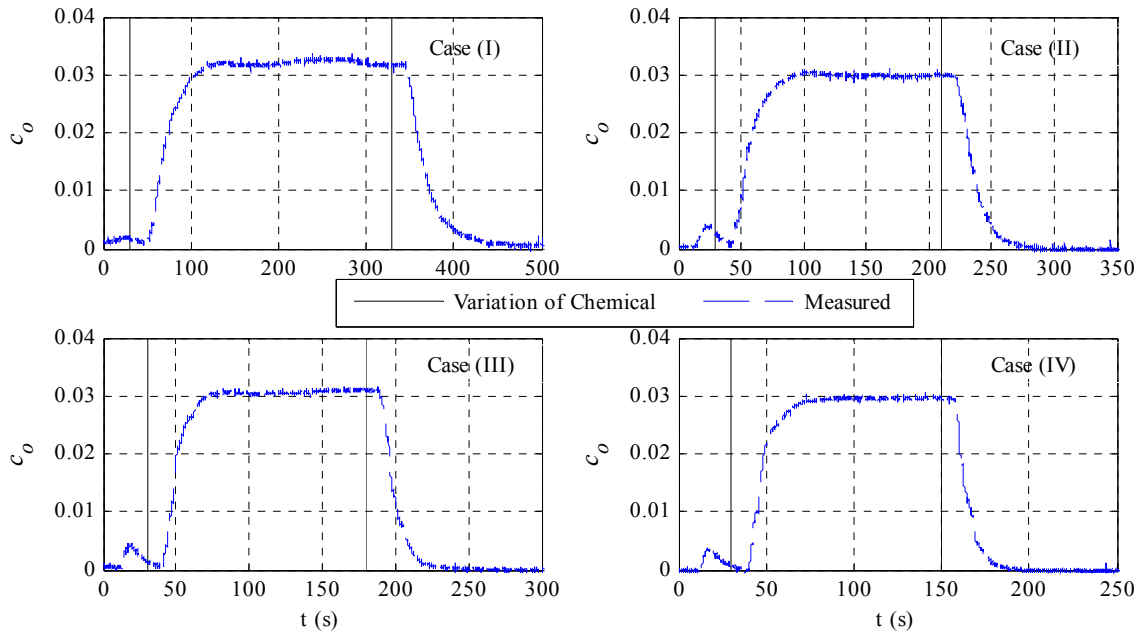


Figure 13. Experimental results for the carrier-chemical mix concentration dynamics c_o defined in equation 26.

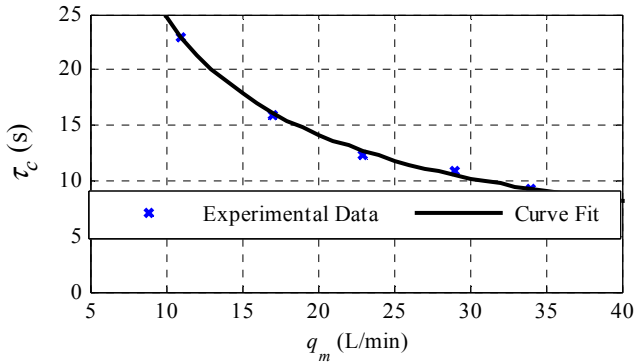


Figure 14. Experimental curve for τ_c vs. q_m found with statistic determination coefficient $R^2=0.99$.

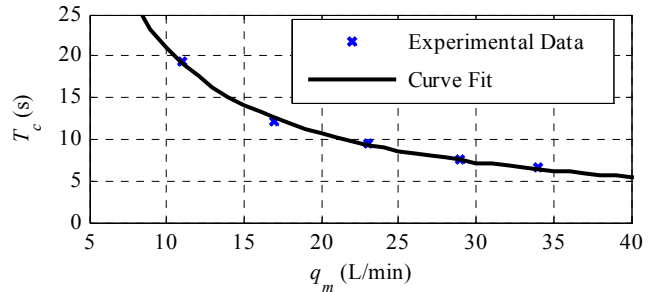


Figure 15. Experimental curve for T_c vs. q_m found with statistic coefficient of determination $R^2=0.99$.

presented in figure 9 which was simulated for the nominal parameters given in table 7.

To validate the carrier-chemical mix concentration model, different values for inputs q_c and q_m were used. These inputs are shown in figure 16 along with the model and experimental results for the concentration c_o . The reference values for q_m and q_c were regulated by a proportional, integral, and derivative (PID) and PI controller, respectively. Both controllers were implemented in the LabVIEW RT software and were run every 50 ms.

It can be seen in figure 16 that the results obtained from the carrier-chemical mix concentration model were close to the actual data. The normalized RMSE value for c_o was

Table 7. Parameters of the carrier-chemical mix concentration model.

Parameter Name and Variable	Value
Coefficient (eq. 30), K	5120
Coefficient (eq. 31), K_1	158
Coefficient (eq. 32), K_2	197
Coefficient (eq. 31), ϕ_1	0.85
Coefficient (eq. 32), ϕ_2	0.97
Minimum value provided by the flow meter, q_-	5.00 L min ⁻¹
Maximum value at the sprayer pump flow, q_+	42.00 L min ⁻¹

0.062 a value much less than one indicating an excellent model performance.

CONCLUSIONS

Mathematical models of the chemical sub-system and the chemical-carrier mix delivery system for a DIS were developed. The mathematical models were developed to simulate more realistic operation of a DIS. An equivalent hydraulic circuit to describe the pressure and the flow dynamics of the sprayer was proposed. In addition, a model for the carrier-chemical mix concentration delivery system was used to estimate the transport delay and the sprayer time response. This model was calibrated from measurements using a conductivity sensor. From this research, we can conclude that:

1. The dynamics of a DIS flow rates q_m and q_c were satisfactorily described by the developed models validated by normalized RMSE values lower than 0.4.

- The mix concentration transport delay and time constant depended on the mixture flow rate (q_m). Both decreased with increasing flow rate according to a power function shape and were estimated with very good performance validated by a coefficient of determination ($R^2=0.99$).
- Experimental results obtained from the test bench built showed that the performance of the sprayer system could be efficiently predicted with the developed models.
- The developed models are useful to design appropriate controllers and to anticipate a map-based rate avoiding under application.

ACKNOWLEDGEMENTS

The authors gratefully acknowledge the financial support of the Conselho Nacional de Desenvolvimento Científico e Tecnológico (CNPq) under grants 143452/2008-8, 479306/2008-7, 304985/2009-0, 306477/2013-0, and Empresa Brasileira de Pesquisa Agropecuária (Embrapa) under projects MP1: 01.09.01.002.01 and MP2 02.11.07.025.00.05.

REFERENCES

- Aissaoui, A. El. (2015). A feasibility study of direct injection spraying technology for small scale farming: Modeling and design of a process control system. PhD diss. Liege, Belgium: University of Liege-Gembloux, Agro-Bio Tech.
- Aissaoui, A. El., Lebeau, F., Elbahir, L., Destain, M.-F., & Houmy, K. (2011). A feasibility study of developing direct injection spraying technology for small scale farms. *Proc. Synergy Tech. Development of Agriculture and Food Industry*, (pp. 1-6). Gödöllő, Hungary: Szent István University
- Aissaoui, A. El., Lebeau, F., Elbahir, L., Destain, M.-F., & Houmy, K. (2009). Applying control volume finite element for modelling direct injection boom spraying flow. *Proc. 7th World Congress on Computers in Agriculture and Natural Resources Conf.* St. Joseph, MI: ASABE.
- Akers, A., Gassman, M., & Smith, R. (2006). *Hydraulic Power System Analysis*. Boca Raton, FL: CRC Press. <http://dx.doi.org/10.1201/9781420014587>
- Antuniassi, U. R., Miller, P., & Paice, M. (2002). Performance evaluation of injection metering systems. *Revista Brasileira de Engenharia Agrícola e Ambiental*, 6(1), 159-165. Retrieved from http://www.scielo.br/scielo.php?script=sci_arttext&pid=S1415-43662002000100028&nrm=iso
- Cruvinel, P. E., Oliveira, V. A., Felizardo, K. R., & Mercaldi, H. V. (2011). Bancada automatizada para ensaios e desenvolvimento de pulverizadores de agrotóxicos, aplicadores de fertilizantes líquidos e maturadores em culturas agrícolas sob manejo baseado em agricultura de precisão (Automated bench for testing and development of pesticide sprayers, liquid fertilizer applicators and maturators in crops under management based on precision agriculture). In R. Y. Inamasu, J. M. Naime, A. V. Resende, L. H. Bassoi, & A. C. C. Bernardi (Eds.), *Agricultura de Precisão: um Novo Olhar* (pp. 96-100). São Carlos, S.P.: Embrapa Instrumentação.
- Downey, D., Crowe, T. G., Giles, D. K., & Slaughter, D. C. (2006). Direct nozzle injection of pesticide concentrate into continuous flow for intermittent spray applications. *Trans. ASABE*, 49(4), 865-873. <http://dx.doi.org/10.13031/2013.21726>
- Ferreira, C. R. r. P. T., Camargo, M. L. B., & Vegro, C. L. R. (2013). Defensivos agrícolas: Vendas batem novo recorde em 2012 e segue em ritmo forte em 2013. *Análises e Indicadores do Agronegócio*, 8(7), 1-5.
- Garcia, C. (2005). *Modelagem e Simulação de Processos Industriais e de Sistemas Eletromecânicos* (2nd ed.). São Paulo, S.P.: EDUSP.
- Gillis, K. P., Giles, D. K., Slaughter, D. C., & Downey, D. (2003). Injection mixing system for boomless, target-activated herbicide spraying. *Trans. ASAE*, 46(4), 997-1008. <http://dx.doi.org/10.13031/2013.13954>
- Hoogterp, A. (2009). Map-based spraying with a direct injection system: Performance measurement of an injection sprayer. MS thesis. Wageningen, Netherlands: Wageningen Universteit, Agricultural and Bioresource Engineering.
- Lammers, P. S., & Vondricka, J. (2008). Evaluation of a carrier control valve for a direct nozzle injection system. *Biosyst. Eng.*, 103(1), 43-48. <http://dx.doi.org/10.1016/j.biosystemseng.2009.02.008>
- Lammers, P. S., & Vondricka, J. (2010). Direct injection sprayer. In E.-C. Oerke, R. Gerhards, G. Menz, & R. A. Sikora (Eds.), *Precision Crop Protection--The Challenge and Use of Heterogeneity*. Dordrecht: Springer Netherlands. http://dx.doi.org/10.1007/978-90-481-9277-9_18
- Luck, J. D., Shearer, S. A., Luck, B. D., & Payne, F. A. (2012). Technical note: Evaluation of a rhodamine-wt dye/glycerin mixture as a tracer for testing direct injection systems for agricultural sprayers. *Appl. Eng. Agric.*, 28(5), 643-646. <http://dx.doi.org/10.13031/2013.42424>
- Manalil, S., Busi, R., Renton, M., & Powles, S. B. (2011). Rapid evolution of herbicide resistance by low herbicide dosages. *Weed Sci.*, 59(2), 210-217. <http://dx.doi.org/10.1614/WS-D-10-00111.1>
- Mercaldi, H. V., Felizardo, K. R., Oliveira, V. A., & Cruvinel, P. E. (2011). Modelagem de um sistema de injeção direta de herbicida em taxa variável para aplicação em culturas agrícolas (Herbicide direct injection system modeling for variable rate application in agricultural fields). In R. Y. Inamasu, J. M. Naime, A. V. Resende, L. H. Bassoi, & A. C. C. Bernardi (Eds.), *Agricultura de Precisão: um Novo Olhar* (pp. 101-105). São Carlos, S.P.: Embrapa Instrumentação.
- Merritt, H. E. (1967). *Hydraulic Control Systems*. New York, NY: John Wiley & Sons.
- National Instruments. (2010). cRIO 9072/3/4: Operation instruction and specification. Austin, TX: National Instruments.
- Ogata, K. (2010). *Modern Control Engineering*. Upper Saddle River, NJ: Pearson Education.
- Shiratsuchi, L. S., & Fontes, J. R. A. (2002). Tecnologia de Aplicação de Herbicidas (Herbicide Application Technology). Planaltina, DF: Empresa Brasileira de Agropecuária.
- Sokefeld, M. (2010). Variable rate technology for herbicide application herbicide application. In E. C. Oerke, R. Gerhards, G. Menz, & R. A. Sikora (Eds.), *Precision Crop Protection -- The Challenge and Use of Heterogeneity* (pp. 335-347). Dordrecht Netherlands: Springer Netherlands. http://dx.doi.org/10.1007/978-90-481-9277-9_21
- Steward, B. L., & Humburg, D. S. (2000). Modeling the raven SCS-700 chemical injection system with carrier control with sprayer simulation. *Trans. ASAE*, 43(2), 231-245. <http://dx.doi.org/10.13031/2013.2698>
- Sui, R., Thomasson, J. A., Willers, J. L., Lee, F. P., & Wang, R. (2003). Variable-rate spray system dynamic evaluation. ASAE Paper No. 031128. St. Joseph, MI: ASAE. <http://dx.doi.org/10.13031/2013.14931>

- Sundaresan, K. R., & Krishnaswamy, P. R. (1978). Estimation of time delay time constant parameters in time, frequency, and Laplace domains. *Canadian J. Chem. Eng.*, *56*(2), 257-262. <http://dx.doi.org/10.1002/cjce.5450560215>
- Tompkins, F. D., Howard, K. D., Mote, C. R., & Freeland, R. S. (1990). Boom flow characteristics with direct chemical injection. *Trans. ASAE*, *33*(3), 737-743. <http://dx.doi.org/10.13031/2013.31394>
- Vondricka, J., Hloben, P., & Lammers, P. S. (2007). Optimization of direct nozzle injection system for site-specific herbicide application. ASABE Paper No. 071085. St. Joseph, MI: ASABE. <http://dx.doi.org/10.13031/2013.22906>
- Zhu, H., Fox, R. D., Ozkan, H. E., Brazee, R. D., & Derksen, R. C. (1998). A system to determine lag time and mixture uniformity for inline injection sprayers. *Appl. Eng. Agric.*, *14*(2), 103-110. <http://dx.doi.org/10.13031/2013.19369>